Tunable band gaps in bilayer transition-metal dichalcogenides

Ashwin Ramasubramaniam*
Department of Mechanical and Industrial Engineering, University of Massachusetts Amherst, Amherst, Massachusetts 01003, USA

Doron Naveh† and Elias Towe‡
Department of Electrical and Computer Engineering, Carnegie Mellon University, Pittsburgh, Pennsylvania 15213, USA
(Received 15 July 2011; revised manuscript received 1 November 2011; published 18 November 2011)

We investigate band-gap tuning in bilayer transition-metal dichalcogenides by external electric fields applied perpendicular to the layers. Using density functional theory, we show that the fundamental band gap of MoS_2, $MoSe_2$, $MoTe_2$, and WS_2 bilayer structures continuously decreases with increasing applied electric fields, eventually rendering them metallic. We interpret our results in the light of the giant Stark effect and obtain a robust relationship, which is essentially characterized by the interlayer spacing, for the rate of change of band gap with applied external field. Our study expands the known space of layered materials with widely tunable band gaps beyond the classic example of bilayer graphene and suggests potential directions for fabrication of novel electronic and photonic devices.

DOI: 10.1103/PhysRevB.84.205325 PACS number(s): 73.21.Ac, 71.20.Nr

I. INTRODUCTION

Layered transition-metal dichalcogenides (TMDs) are an intriguing family of materials that span a broad range of physical properties and have been extensively studied for applications in catalysis, tribology, electronics, photovoltaics, and electrochemistry.[1–4] There has been a renewal of interest in the properties of TMDs, especially in their 2D crystalline form, in the wake of extensive research on graphene.[5] Recent experiments have demonstrated that TMDs provide a rich source of two-dimensional crystals[6,7] with potential applications in nanoelectronics and nanophotonics.[8–11] For example, monolayer MoS_2 based transistors have been found to display mobilities approaching graphene nanoribbons, accompanied by high on-off ratios.[10] While the inherent band gap of monolayer MoS_2 ($\sim$1.9 eV[9]) obviates the need for band-gap engineering in these devices—an unavoidable and vexing problem in the case of graphene, which is a semimetal in its pristine state—the ability to manipulate the band gap of TMDs could lead to new functionalities in these materials.

Among several strategies currently being employed to engineer band gaps in graphene, band-gap tuning by external electric fields in bilayer graphene[12–15] is a particularly interesting one. An external electric field applied normal to the graphene sheets breaks the inversion symmetry of the bilayer structure and opens up a band gap. Remarkably, this gap is reversible and continuously tunable up to about 250 meV.[13] Recent theoretical studies also suggest the possibility of employing a similar strategy to manipulate the band gap in bilayer hexagonal boron nitride;[16] in this case, an external electric field *reduces* the fundamental band gap of the bilayer structure, although it would appear that rather large fields ($\geqslant$6 V/nm) would be required to induce a complete semiconductor-metal transition. Other theoretical studies on boron nitride nanoribbons[17,18] have also shown the potential for band-gap tuning by externally applied in-plane electric fields. There have also been earlier theoretical investigations on band-gap tuning of boron nitride nanotubes via external electric fields by Louie and coworkers.[19] Those authors showed that transverse electric fields can be used to significantly modulate the band gaps of boron nitride nanotubes and, in some instances, even render them metallic. In analogy with the familiar atomic Stark effect, they dubbed this phenomenon the giant Stark effect (GSE). Their predictions were experimentally confirmed by Ishigami *et al.*[20] In light of these preceding studies, it is natural to inquire whether similar strategies for band-gap tuning can be employed in TMD nanostructures. We address this question in the context of bilayer TMDs in this paper.

In the following, we present density functional theory (DFT) calculations that elucidate the electronic properties of bilayer TMD structures under the application of an external electric field normal to the sheets. This configuration is an idealization of a bilayer TMD device sandwiched between a substrate and a top-gate dielectric (without the attendant complication of additional material interfaces). As a representative set of layered TMDs, we consider MoS_2, $MoSe_2$, $MoTe_2$, and WS_2, all of which are semiconductors with band gaps of 1–1.5 eV in their bulk state.[21,22] We show that by applying increasing electric fields normal to bilayers of these materials, their fundamental gaps can be continuously driven to zero. This is noteworthy since the range of gap tunability is significantly larger than bilayer graphene ($\sim$250 meV). Furthermore, we find that typical external fields required to induce the semiconductor-metal transition are in the range of 2–3 V/nm as compared to the rather large values ($\geqslant$6 V/nm) reported for hexagonal boron nitride.[16] We also present a simple analytical model and a robust relationship for the rate of band-gap change with applied electric field, which should be testable experimentally. In light of our findings, it would appear that bilayer TMDs could significantly expand the known space of layered materials with widely tunable band gaps beyond bilayer graphene and provide further avenues for novel nanoelectronics and photonics applications.

II. RESULTS AND DISCUSSION

MoS_2, $MoSe_2$, $MoTe_2$, and WS_2 commonly crystallize in the $2H_b$ polytype. As seen from Fig. 1, each molecular sheet consists of a chalcogen-metal-chalcogen sandwich structure,

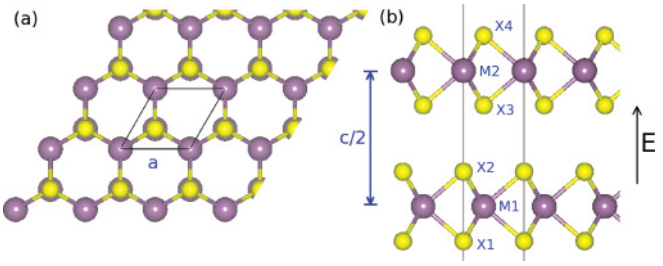

FIG. 1. (Color online) Schematic of the $2H_b$ MX_2 (M = Mo, W; X = S, Se, Te) bilayer structure: (a) top and (b) side views. The metal and chalcogen atoms are represented by large purple and small yellow spheres, respectively. The unit cell is enclosed by black lines. Electric fields are applied normal to the sheets along the positive c axis.

with trigonal prismatic coordination of the metal atoms.[1,21] Consecutive sheets are laterally offset such that the transition-metal (TM) atoms of one layer are above the chalcogen atoms of the other layer; the sheets only interact with each other through weak van der Waals forces. It is known that standard DFT with semilocal functionals (LDA/GGA) fails to describe such weak nonlocal interactions correctly.[23] Therefore in the model used for our calculations, we constrain the spacing between the TM-TM layers to their experimentally determined bulk value (Table I). We do not expect this procedure to affect the overall conclusions.[50] The in-plane lattice vector a was also fixed at the experimental value. The positions of the chalcogen atoms alone were relaxed with a force tolerance of 0.001 eV/A at zero field; all atomic positions were kept fixed thereafter (see further discussion in the Appendix). Post-relaxation electronic structure calculations were performed with spin-orbit coupling. Additional computational details are provided in the methods section at the end of the paper.

In Fig. 2, we provide an overview of the band structures of the various TMD bilayers considered in this work as a function of applied external field. It is apparent at a glance that the band gap in all cases is driven continuously to zero with increasing external fields. We note that in all cases, the fundamental band gap at zero external field is an indirect gap between the valence-band (VB) maximum at Γ and the conduction-band (CB) minimum, which lies between Γ and K.[25] The application of an external field shifts the CB minimum to the K point, with the exception of WS_2. The effect on the VB maximum is more material specific. For $MoSe_2$ and $MoTe_2$, the VB maximum shifts to the K point; with increasing electric fields, gap closing occurs at the K point. For MoS_2, the VB maxima at Γ and K inexorably approach the same value with increasing external fields. At the semiconductor-metal transition, these two maxima are near degenerate to within the error of the numerical method and so we cannot definitively assert whether the gap closing is direct at K or indirect between Γ and K. For WS_2, the gap closing is indirect between the VB maximum at K and the CB minimum intermediate between Γ and K. To attain more insight into the physical mechanisms underlying the electric-field-induced semiconductor-metal transition in these TMD bilayers, we now proceed to perform a more detailed electronic structure analysis. For brevity, we will use MoS_2 as a generic example, which is sufficient to illustrate the broader trends for the other TMDs as well.

TABLE I. Structural parameters a and c (indicated in Fig. 1) for the $2H_b$ polytypes of MoX_2 (Ref. 21) and WS_2 (Ref. 24) employed in the DFT calculations. Also listed are the metal-chalcogen bond lengths d_{Mi-Xj} (see Fig. 1) obtained from atomic relaxation. All distances are in Å.

	MoS_2	$MoSe_2$	$MoTe_2$	WS_2
a	3.160	3.299	3.522	3.153
c	12.294	12.938	13.968	12.323
d_{M1-X2}, d_{M2-X3}	2.406	2.536	2.727	2.409
d_{M1-X1}, d_{M2-X4}	2.411	2.542	2.731	2.415

The electronic structure of bulk MoS_2 has been thoroughly investigated via experiments and theory.[1,9,11,21,25–28] The electronic states near the Fermi level are dominated by Mo $4d$ and S $3p$ levels. The occupied part of the d band consists of mixed Mo d_{xy}-$d_{x^2-y^2}$ character in addition to significant d_{z^2} character. At Γ, there is also appreciable S p_z character. At K, the occupied part of the d band has dominant d_{xy}-$d_{x^2-y^2}$ character whereas the unoccupied portion is dominated by d_{z^2} character.[26] The VB maximum is located at the Γ point while the CB minimum is located about halfway between Γ and K; the gap is thus indirect and of the order of 1.3 eV.[9,11] The states originating from mixing of Mo d_{z^2} orbitals and the S p_z orbitals at Γ are fairly delocalized and have an antibonding nature. On increasing the separation between consecutive MoS_2 layers, the layer-layer interaction decreases and lowers the energy of the antibonding states; consequently, the VB maximum at Γ shifts downward.[25] The states at K which are of d_{xy}-$d_{x^2-y^2}$ character are mostly unaffected by interlayer spacing. Thus, in the limit of widely separated planes, i.e., monolayer MoS_2, the material becomes a direct gap semiconductor with a gap of about 1.9 eV at K.[9]

The band structure and the atom-projected partial density of states (PDOS) decomposed by azimuthal and magnetic quantum number (lm-decomposed PDOS) for bilayer MoS_2 are displayed in the topmost row of Fig. 3. A noteworthy feature of the band structure is the splitting of the valence band at K (marked by up and down arrows in Fig. 3) by 0.17 eV. Note that since the calculations are performed with spin-orbit coupling, each of these split levels is actually composed of two singly occupied levels that are essentially degenerate (∼5 meV difference) within the accuracy of the calculations. This valence-band-splitting at K is well known from studies of bulk samples and is attributed to a combination of spin-orbit splitting and interlayer interactions.[1,27] Excitations from this split valence band to the conduction band at K are responsible for the so-called A and B excitons.[1] The exciton splitting in bulk samples was experimentally measured to be 0.16 eV by Coehoorn *et al.*[27] and 161 ± 10 meV by Böker *et al.*;[21] the latter authors also performed DFT calculations and obtained a splitting of 258 meV. For the bulk sample, we find a corresponding splitting of 0.23 eV (see Fig. 7) in reasonable agreement with the cited values. The partial charge densities from the HOMO and LUMO at important points (Γ and K) are displayed in Fig. 4 to facilitate easy identification of the orbital contributions at these points. The inversion symmetry

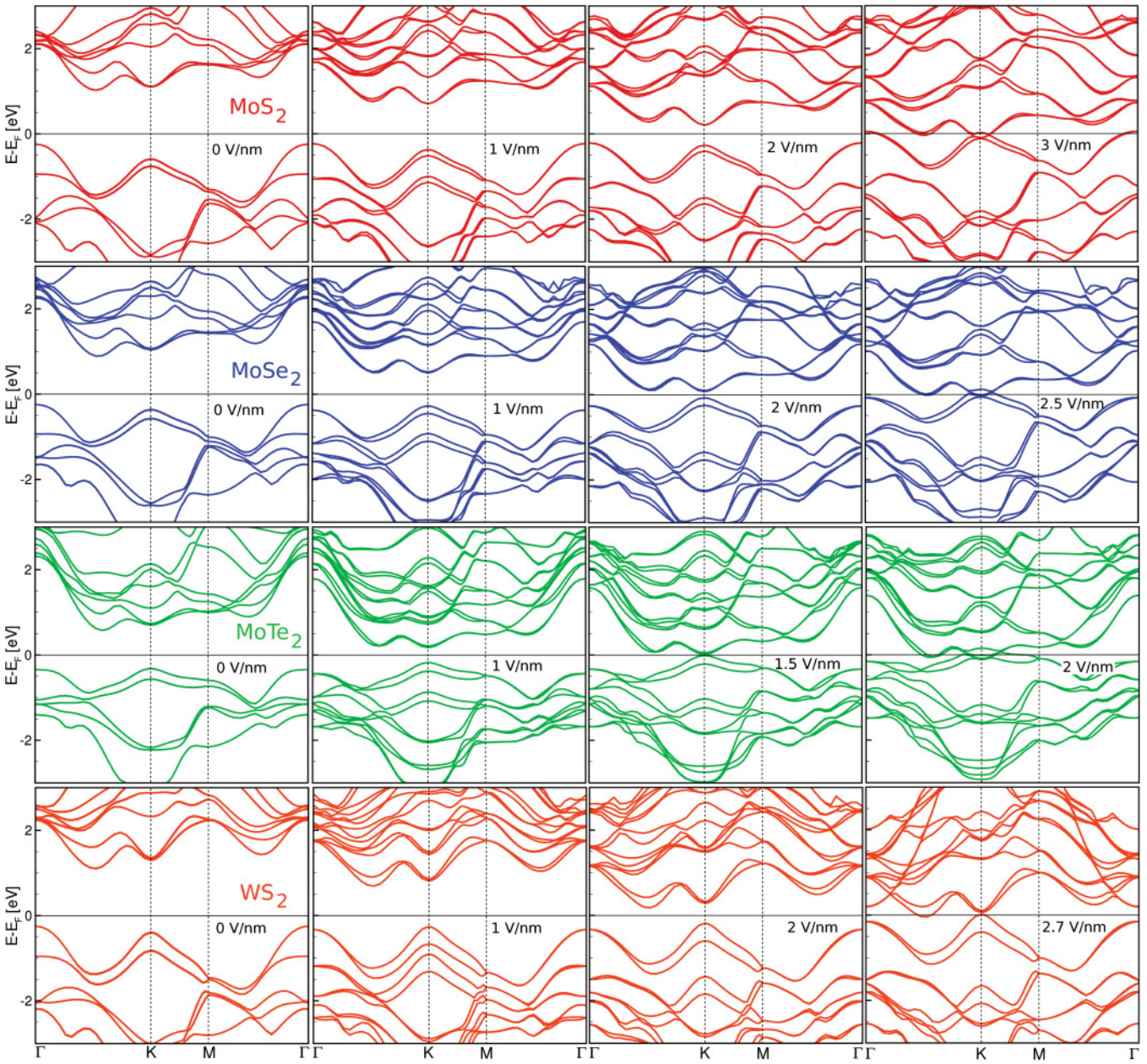

FIG. 2. (Color online) Band structure along Γ-K-M-Γ direction in reciprocal space as a function of applied external electric field. For MoX_2 compounds, the fundamental band gap at zero field is indirect between the VB maximum at Γ and the CB minimum, which lies between Γ and K. Application of an external field alters the positions of the VB maximum and CB minimum, the details being material specific. For MoS_2, the VB maxima at Γ and K are nearly equal in value (to within the error of the calculation) and thus it is not possible to clearly identify whether the gap closing is indirect between Γ and K or direct at K. For $MoSe_2$ and $MoTe_2$, the gap closing is clearly direct at K. For WS_2, the zero-field gap is initially between the VB maximum at Γ and the CB minimum, which lies between Γ and K. Upon application of an external field, the CB minimum still remains between Γ and K, but the VB minimum shifts from Γ to K; the gap closes eventually between these points.

of the bilayer structure about its midplane is reflected in the identical PDOS signature of the two Mo atoms, S atoms S2 and S3 (internal to the bilayer structure), and S atoms S1 and S4 on the vacuum sides of the slab. The HOMO at Γ is composed primarily of Mo d_{z^2} states and p_z orbitals from S2 and S3. Due to the presence of vacuum on the S1 and S4 sides, these p_z orbitals do not interact with antibonding orbitals on S atoms from the neighboring layer; thus the states are lower in energy and make smaller contributions to the HOMO at Γ. At K, the HOMO is primarily of d_{xy}-$d_{x^2-y^2}$ character while the LUMO is primarily of d_{z^2} character; in both cases there is always some mixing between the d_{xy}-$d_{x^2-y^2}$ and d_{z^2} bands.

Upon application of an external field, the valence and conduction subband states separately undergo mixing leading to a field-induced splitting of the electronic levels.[18–20] The analogy with the familiar atomic level Stark effect is immediate, which led to this phenomenon being dubbed the giant Stark effect (GSE) by Louie and coworkers.[19] The consequences of

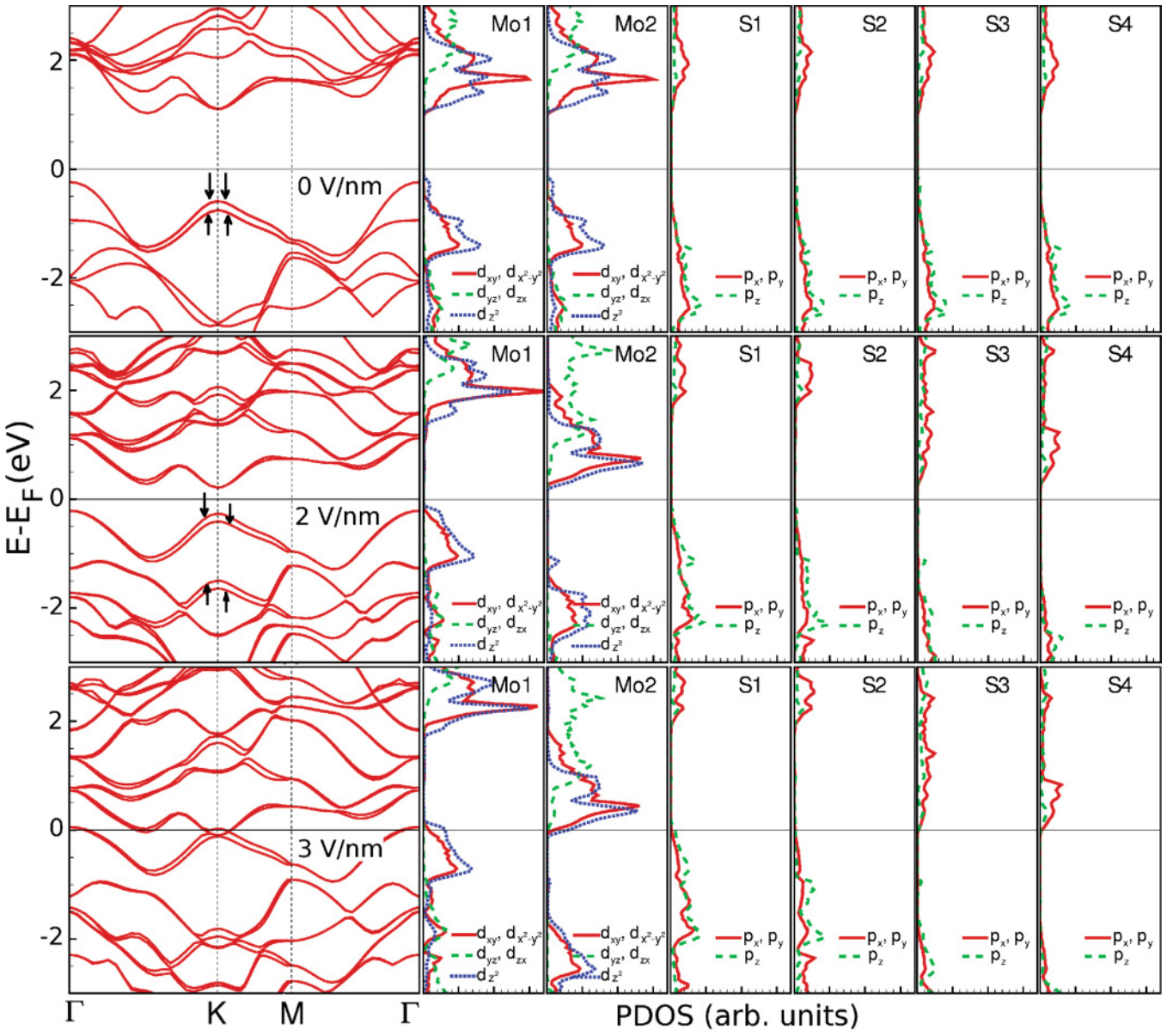

FIG. 3. (Color online) Band structure along Γ-K-M-Γ direction in reciprocal space and lm-decomposed atom-projected density of states (PDOS) as a function of applied external electric field for bilayer MoS_2. The atom labels for the PDOS plots are indicated in Fig. 1. The two layers are degenerate, as expected, at zero fields. Application of an external electric field breaks inversion symmetry between the layers localizing the HOMO and LUMO on the lower and upper layers, respectively.

the GSE are twofold. First, field-induced repulsion among the electronic levels leads to an upshift of the VB edge and a downshift of the CB edge leading to a decrease in the band gap (Fig. 3). Second, due to splitting of the electronic levels, the HOMO and LUMO, which were initially distributed over both layers, are now mostly localized on the bottom and top layers, respectively, as clearly seen in Fig. 4. As an analogy, in the case of boron nitride nanotubes under transverse fields, the HOMO and LUMO localize on opposite sides of the diameter;[19] for nanoribbons under a transverse field, they localize on opposite edges.[17,18] As the electric field is continuously increased, the gap eventually closes and renders the structure metallic. It is interesting to note from both the band structure and the density of states in Fig. 3 that, to a reasonable approximation, the valence and conduction bands are rigidly translated toward the Fermi level with increasing electric fields. We will exploit this observation subsequently in constructing a simple two-band model for estimating the rate of change of the band gap with applied field. It is also worth noting that the initially degenerate uppermost levels of the valence band are also split by the electric field (contrast positions of similar arrows in Fig. 3) by 0.1–0.14 eV over the range of electric fields applied here.

To facilitate a closer inspection of charge redistribution within the bilayer structure, we display in Fig. 5 the charge-density difference plots $[\rho(E) - \rho(0)]$ at increasing magnitudes of the external electric field E. We see that there is a progressive depletion of charge density in the sulfur (S) p_z orbitals as well as in the bonding region between the

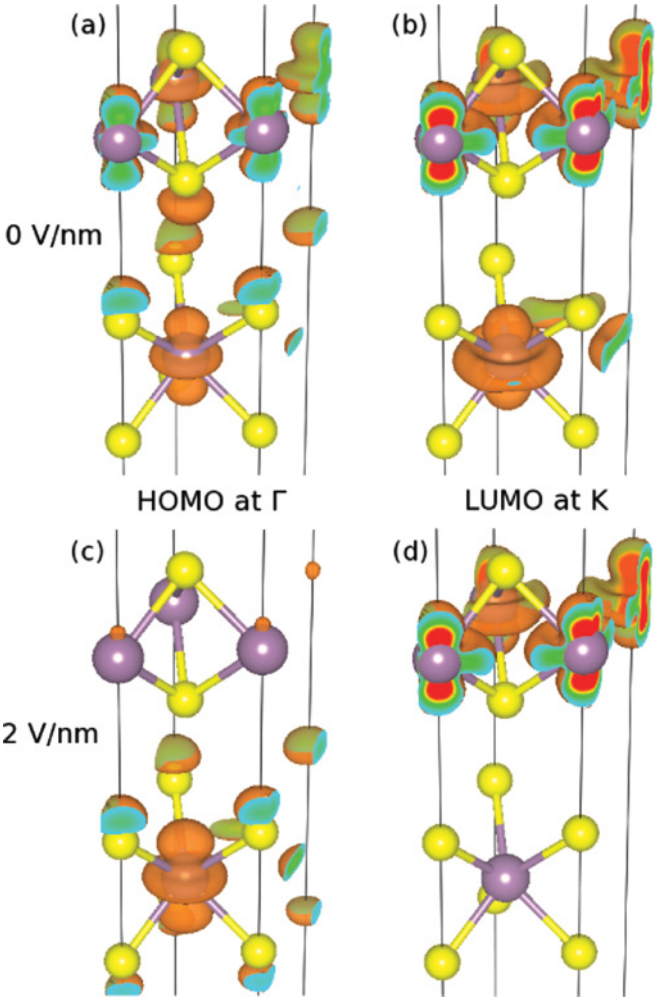

FIG. 4. (Color online) Partial charge density from the HOMO at Γ [(a), (c)] and the LUMO at K [(b), (d)] at external fields of 0 V/nm (upper row) and 2 V/nm (lower row). All isosurfaces are at 0.05 $e/\text{Å}^3$. At zero electric field inversion symmetry of the layers is preserved. The HOMO at Γ is primarily of Mo d_{z^2} and S p_z character with smaller contributions from Mo d_{xy} and $d_{x^2-y^2}$. The LUMO at K is also primarily of Mo d_{z^2} in character with smaller contributions from Mo d_{xy} and $d_{x^2-y^2}$. An external field of 2 V/nm external fields clearly breaks symmetry between the MoS_2 layers, localizing the HOMO and LUMO on different layers.

Mo and S atoms with increasing electric field. Conversely, there is an accumulation of charge density in the Mo d_{xy}, $d_{x^2-y^2}$, and d_{z^2} orbitals, in the sulfur (S) p_x and p_y orbitals, as well as in the interlayer space between the MoS_2 sheets. In essence, the external electric field *localizes* charge along the direction of the applied field, confining charge to atomic planes, but *delocalizes charge within these planes*, thereby driving the semiconductor-metal transition in bilayer MoS_2. For completeness, it is also worth noting that we did not observe similar band-gap modulation in monolayer MoS_2; electric fields of similar magnitude merely induced small shifts and deformation in the band structure.

The basic mechanism of the semiconductor-metal transition outlined above also holds for $MoSe_2$, $MoTe_2$, and WS_2; for detailed band-structure and charge-density difference plots, see Figs. 1– 4 of the Supplemental Material.[29] As a general

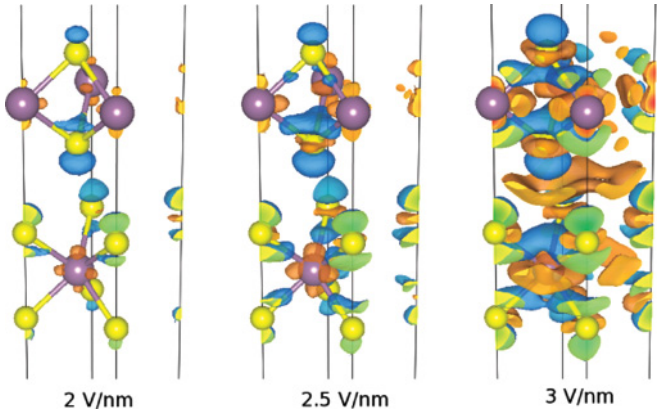

FIG. 5. (Color online) Charge density *difference* between bilayer MoS_2 at nonzero and zero external field. Orange and blue isosurfaces correspond to positive and negative values of 5.4×10^{-4} $e/\text{Å}^3$, respectively. As the electric field increases in going from left to right, we see progressive depletion of charge density in the S p_z orbitals and in the bonding region between the Mo and S atoms. Correspondingly, there is an accumulation of charge density in the S p_x and p_y orbitals as well as the Mo d_{xy}, $d_{x^2-y^2}$, and d_{z^2} orbitals.

trend for MoX_2 bilayers, we see that the critical electric field for the semiconductor-metal transition decreases in going from S to Se to Te. We attribute this to the increasingly diffuse nature of the valence p_z orbitals in going from S to Te, which facilitates greater charge transfer from the chalcogen to Mo at the same level of electric field. The effect of switching the transition metal from Mo to W while retaining the chalcogen (S) is not significant: The semiconductor-metal transition occurs at about the same applied field for MoS_2 and WS_2. Figure 6 summarizes the results for band-gap (E_g)

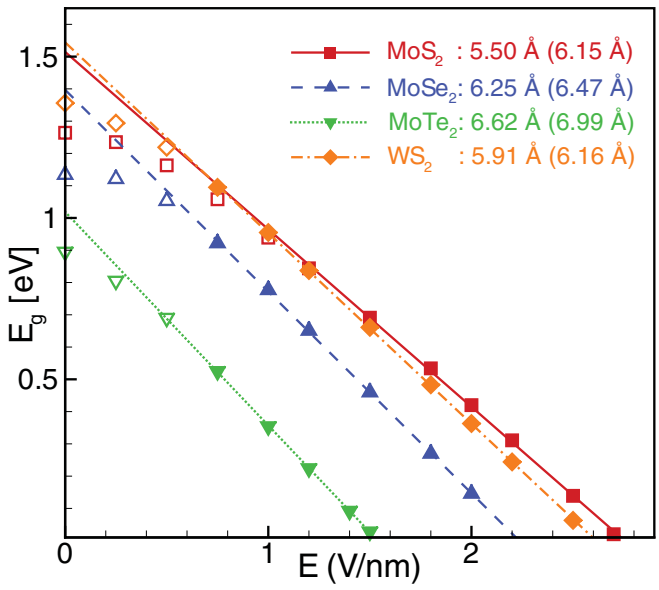

FIG. 6. (Color online) Band gap E_g versus applied electric field E for MoS_2, $MoSe_2$, $MoTe_2$, and WS_2. The lines are fits to the linear portion of the curve indicated by solid symbols. Hollow symbols are within the region of nonlinear response and are excluded from the fits. The GSE coefficients (magnitudes of the slopes of the linear fits) are indicated; interlayer spacings are in parentheses.

versus applied electric field (E) for the different bilayer TMDs considered here. The initial response of the band gap to the applied field is nonlinear (likely quadratic) with zero slope at $E = 0$ (from symmetry considerations). For larger fields, the response is linear and the slope of the curve can be described as

$$\frac{dE_g}{dE} = -e\mathcal{S}, \tag{1}$$

where e is the electron charge and $\mathcal{S}$ is the linear GSE coefficient. Following Zheng *et al.*,[18] since the potential of the applied electric field is eEz, the change in the band gap is approximately

$$\Delta E_g = eE\langle z\rangle_{cb} - eE\langle z\rangle_{vb}, \tag{2}$$

where $\langle z\rangle_{cb(vb)}$ represents the center of the conduction (valence) band along the direction of the applied field. This essentially amounts to assuming a two-band model in which the valence and conduction bands undergo rigid shifts (in opposite directions) in response to the applied electric field; Fig. 3 seems to corroborate this point of view, as noted before. From Eqs. (1) and (2) it follows that $\mathcal{S} = \langle z\rangle_{vb} - \langle z\rangle_{cb} \approx c/2$, since the HOMO and LUMO localize on different layers. From the fitted slopes in Fig. 6, it is clear that $\mathcal{S}$ does indeed scale with the interlayer separation and, moreover, is fairly close to that actual interlayer separation ($c/2$).

In concluding this section, a final remark about band gaps and critical fields for the semiconductor-metal transition are in order. First, with respect to band gaps, it is well known that semilocal [local density approximation (LDA) / generalized gradient approximation (GGA)] exchange-correlation (XC) functionals typically underestimate experimental band gaps.[30] Hybrid functionals, which incorporate a portion of exact Hartree-Fock exchange, generally tend to be more accurate in this regard,[31] as do many-body techniques such as the GW method,[32] but the degree of improvement (or lack thereof) can be material specific.[33] A detailed study of the sensitivity of the electronic structure to the choice of XC functional and/or technique is well beyond the scope of this work; a general idea of the trends can be anticipated though, specifically for MoS_2 for which there exist previous comparative studies. For bulk MoS_2 Botti *et al.*[34] report PBE, PBE0, and HSE06 gaps of 0.87 eV, 2.09 eV, and 1.42 eV, respectively—the experimentally measured gap is 1.29 eV.[35] PBE underestimates the gap, as expected, while both hybrids (PBE0 and HSE06) overestimate the gap. For monolayer MoS_2, Mak *et al.*[9] measured a direct gap of 1.90 eV via optical spectroscopy. Li and Galli[25] employed the PW91 GGA functional in plane-wave DFT calculations and reported a direct gap of 1.8 eV; Botello-Mendez *et al.*[36] employed an LDA functional and DFT with a local basis set and reported a gap of 1.8 eV; Lebègue and Eriksson[37] employed the PBE GGA functional in VASP and obtained a direct gap of 1.78 eV. Ataca and Ciraci[38] report an HSE06 gap of 2.23 eV, a G_0W_0 gap of 2.78 eV, and a GW_0 gap of 2.5 eV. In short, discrepancies between experimental and computational estimates of the gap still exist even when more sophisticated techniques beyond standard LDA/GGA-based DFT are employed. We are unaware of systematic investigations of this kind for bilayer MoS_2. We emphasize that our goal here is *not* to determine precise band gaps but to illustrate the phenomenon of gap-tuning by external fields and to uncover the underlying physics. We suggest that the final test of our predictions will come from experiments, as always; resorting to additional levels of theory to determine precise values of band gaps might or might not shed any further light on the matter given the scatter in data noted above even for the simplest cases with no externally applied fields. We do expect though that the rate of band-gap change with respect to the applied field ($\mathcal{S}$), although estimated here with a simple model, ought to be a robust, theory-independent, experimentally testable prediction. Second, the precise value of the critical field for the semiconductor-metal transition is also expected to be theory dependent—the systematic underestimation of band gaps by semilocal functionals would imply that our estimates for critical fields are lower bounds. However, the decreasing trend in the critical field in going from lighter to heavier chalcogens (keeping the metal species fixed) ought to also be another robust prediction as this only has to do with the fact that the chalcogen valence p_z orbitals become increasingly more diffuse, as discussed before.

III. SUMMARY

In summary, we have shown that external electric fields, which have proven to be a viable tool for band-gap engineering in bilayer graphene, can also be used to tune band gaps in bilayer MoS_2, $MoSe_2$, $MoTe_2$, and WS_2. In contrast to bilayer graphene, where the electric field opens up a gap that saturates at about 0.25 eV,[39] it is possible to *close* the much larger gap of about 1 eV in these bilayer TMDs at similar external fields in the range of 2–3 V/nm. This gap-tuning effect can be interpreted in the light of the giant Stark effect and yields a robust relationship, which is essentially characterized by the interlayer spacing, for the rate of change of band gap with applied external field. Our study expands the known space of layered materials with widely tunable band gaps beyond bilayer graphene and suggests possibilities for novel electronics and photonics applications using TMDs. Given recent success in fabricating monolayer[9,10] and bilayer[9] MoS_2 based devices, we hope to motivate additional experiments along the lines proposed here.

IV. METHODS

DFT calculations including spin-orbit coupling were performed using the Vienna *Ab Initio* Simulation Package

TABLE II. In-plane lattice parameter a and interlayer spacing (between metal layers) $c/2$ for MoS_2 from experiment, PBE-D2 calculations, and PBE calculations, for bulk and bilayer MoS_2. Also listed are the Mo-S bond lengths $d_{\mathrm{Mo}i-\mathrm{S}j}$ (see Fig. 1); for the experimental structure, only S atoms were relaxed with a and c held fixed. All distances are in Å.

	Bulk			Bilayer	
	Expt.	PBE-D2	PBE	PBE-D2	PBE
a	3.160[21]	3.196	3.189	3.199	3.189
$c/2$	6.147[21]	6.218	6.888	6.180	6.760
$d_{\mathrm{Mo1-S2}}$, $d_{\mathrm{Mo2-S3}}$	2.406	2.416	2.417	2.417	2.416
$d_{\mathrm{Mo1-S1}}$, $d_{\mathrm{Mo2-S4}}$	2.406	2.416	2.417	2.417	2.416

(VASP).[40] Core and valence electrons were described using the projector-augmented wave method.[41,42] Semicore p states were also treated as valence states for Mo and W. Electron exchange and correlation (XC) was treated using the generalized gradient approximation as parameterized by Perdew, Burke, and Ernzerhof.[43] Positions of chalcogen atoms were relaxed using a conjugate gradient algorithm with a force tolerance of 0.001 eV/Åwhile the in-plane cell vectors and transition metal–transition metal layer spacing were fixed at the experimental values (Table I). Electronic minimization was performed with a tolerance of 10^{-4} eV and electronic convergence was accelerated with a Gaussian smearing of the Fermi surface by 0.05 eV. The kinetic energy cutoff was set at 400 eV. A $11 \times 11 \times 1$ Monkhorst-Pack mesh, which is sufficient to ensure energy convergence to 1 meV, was used for relaxation calculations; a $31 \times 31 \times 1$ Monkhorst-Pack mesh was used post-relaxation for generating accurate charge densities and density of states. The self-consistent charge densities from the post-relaxation calculations were employed to perform subsequent non-self-consistent, spin-orbit coupling calculations.[44] The cell size was set to 40 Å normal to the bilayer structure to prevent spurious interactions between periodic images of the slabs; for MoS_2, a 30 Å cell was found to be sufficient. Finally, electric fields were applied normal to the slabs, which is accomplished in VASP by introducing dipolar sheets at the center of the simulation cell.[45] Charge-density plots were prepared using VESTA.[46]

ACKNOWLEDGMENTS

A.R. gratefully acknowledges new faculty startup funding from the University of Massachusetts. D.N. and E.T. acknowledge partial financial support of the Army Research Office and the National Science Foundation.

APPENDIX: INFLUENCE OF STRUCTURAL PARAMETERS ON BAND STRUCTURE AND BAND-GAP TUNING

In the calculations presented in the main article, it was noted that the spacing between metal-atom layers as well as the in-plane lattice vector were kept fixed at the experimentally determined values. Furthermore, the atomic positions of the chalcogen atoms were kept fixed after relaxation at zero external field. We discuss the implications of these choices on the computed electronic structure and the predicted giant Stark effect, once again in the context of MoS_2.

First, we examine the effect of lattice parameters on the band structure of bulk MoS_2. All calculations are performed with an energy cutoff of 400 eV, a Gaussian smearing of 0.05 eV, a force tolerance of 0.01 eV/Å, and a $11 \times 11 \times 3$ Monkhorst-Pack mesh. The experimental gap for bulk MoS_2 is 1.29 eV[35] and is indirect[9,21,26–28] between the VB maximum at Γ and the CB minimum along the Γ-K line. The direct gap at K (A exciton energy) is 1.88 eV[27] while the top of the VB at K is estimated to be 0.5 eV below the VB maximum at Γ from the experimental data in Fig. 10 of Ref. 21. Therefore, the CB minimum along the Γ-K line is estimated to be 0.09 eV below the CB minimum at K. In Fig. 7(a) we display the computed band structure for bulk MoS_2 at the experimental lattice parameters ($a = 3.160$ Å and $c = 12.294$ Å) using the PBE XC functional. The gap is indirect between the VB maximum Γ and the CB minimum between Γ and K, and is computed to be 0.87 eV. The difference between the CB minimum along the Γ-K line and the CB minimum at K is 0.25 eV, which is nearly three times higher than our estimate of 0.09 eV from the experimental data. In Fig. 7(b) we display the band structure for bulk MoS_2 obtained after a full relaxation of atomic positions and cell vectors using the PBE XC functional with Grimme's semiempirical dispersion potential (PBE-D2 method).[47] The relevant parameters can be found in the original publication or in the VASP manual.[48] The only modification we made here was to reduce the cutoff distance for long-range interactions from the default value of 30 Å to 15 Å to prevent interactions across vacuum in the cell for the bilayer case (discussed subsequently). This decrease in the cutoff has no substantial effect on the lattice parameters, which we obtain to be $a = 3.196$ Å and $c = 12.436$ Å; Bučko *et al.*[49] report values of $a = 3.19$ Å and $c = 12.42$ Å using the same method, albeit with a long-range cutoff of 30 Å and different energy cutoffs and k-point sampling. Additional structural details are reported in Table II. Bučko *et al.* also report the tendency of the PBE-D2 method to overestimate the cohesive energy (−5.37 eV/atom) unlike PBE (−5.12 eV/atom), which is closer to the experimental estimate (−5.18 eV/atom). As far as the band structure is concerned,

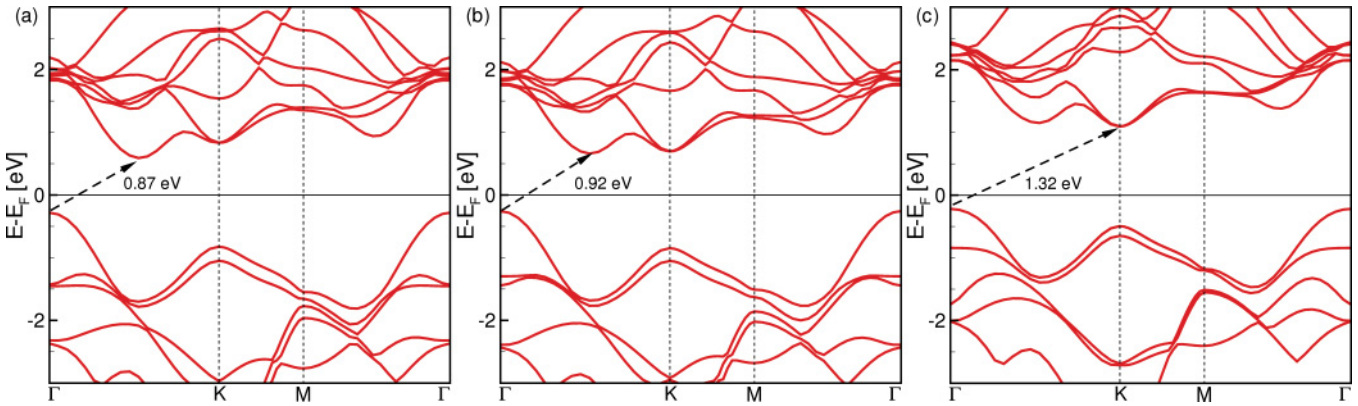

FIG. 7. (Color online) Band structure for bulk MoS_2 at (a) experimental lattice parameters, (b) after relaxation with PBE-D2 method, and (c) after relaxation with PBE.

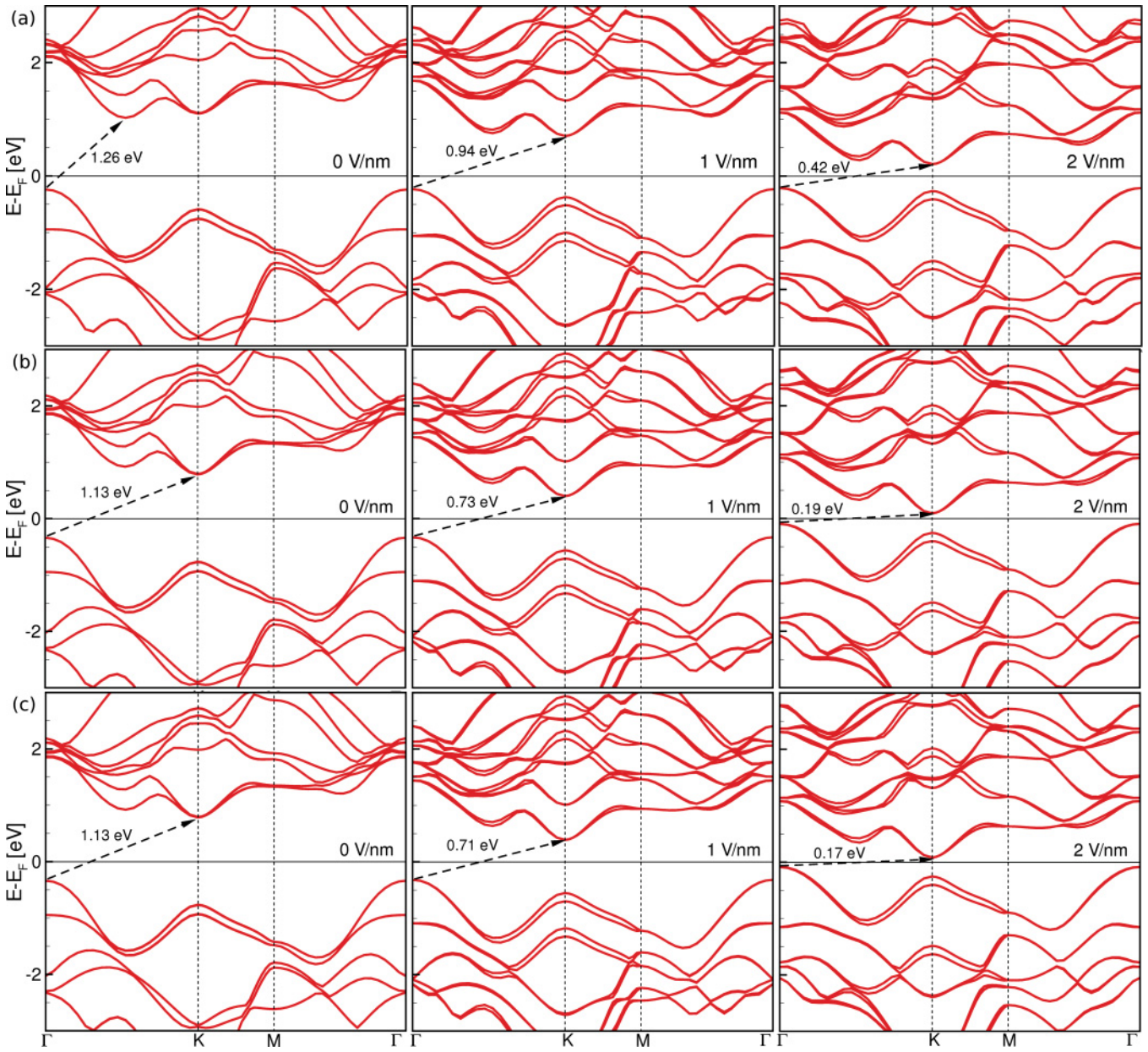

FIG. 8. (Color online) Band structure as a function of applied field for bilayer MoS_2 at (a) experimental lattice parameters (chalcogen atoms relaxed at zero field and kept fixed thereafter), (b) relaxation of entire structure with PBE-D2 method at each applied field, and (c) relaxation of entire structure with PBE-D2 method at zero field (atoms kept fixed thereafter).

the gap is still indirect between the VB maximum at Γ and the CB minimum between Γ and K, and is computed to be 0.92 eV. However, the difference between the CB minimum between Γ and K and the CB minimum at K is 0.034 eV, which underestimates the estimated experimental value of 0.09 eV by a factor of three. Finally, in Fig. 7(c) we display the band structure for bulk MoS_2 obtained after a full relaxation of atomic positions and cell vectors using the PBE XC functional alone. As expected, the in-plane lattice parameter is mostly unaffected ($a = 3.189$ Å) but the interlayer spacing is significantly overestimated ($c = 13.776$ Å). Moreover, the band gap is now indirect between the VB maximum at Γ and the CB minimum at K, in contradiction with all experimental evidence. Overall, it would appear that the role of the interlayer spacing (equivalently, lattice parameter c) is paramount in determining the position of the CB minimum correctly. It would appear that constraining the lattice parameters at the experimental values is a perfectly reasonable strategy for *bulk* MoS_2 as is using semiempirical dispersion corrections.

Next, we consider the bilayer sample. In Fig. 8(a), we repeat the results from Fig. 2 ($a = 3.160$ Å, interlayer spacing $d_{\mathrm{Mo-Mo}} = c/2 = 6.147$ Å; chalcogens relaxed at zero field) for purposes of comparison. The middle row [Fig. 8(b)] displays results obtained for full relaxation (atomic positions and cell vectors) at each applied field using the PBE-D2 method. First, the range of variation in the Mo-Mo layer spacing over the range of fields applied here is ∼0.02 Å while that for the in-plane lattice parameter is ∼0.003 Å. These

variations are small enough to be attributable to tolerances in structural convergence rather than being indicators of any significant coupling between the electric field and van der Waals interactions between the sheets. Second, the PBE-D2 method predicts a larger lattice parameter $a = 3.199$ Å and a larger interlayer spacing $d_{\mathrm{Mo-Mo}} = c/2 = 6.180$ Å (at zero field). Since the interlayer spacing is larger, the CB minimum shifts to the K point and the gap is now 0.92 eV. In contrast, the experimental study of Mak *et al.*[9] reports a direct transition (between VB and CB at K) in the photoluminescence spectra for bilayer MoS_2 at 1.88 eV and an indirect transition between Γ and the CB minimum along the Γ-K line at 1.6 eV. The PBE-D2 band structure therefore appears to be *qualitatively inconsistent* with the experimental observations. In contrast, the band structure at the experimental structural parameters is qualitatively consistent with observations and would appear to be a better choice for computations. Note that the overall concept of band-gap tuning by external fields and the observation of the giant Stark effect is *still valid* irrespective of whether one performs the calculations with PBE at experimental lattice parameters or PBE-D2 at optimized lattice parameters, as evidenced from the trends with increasing external fields in Fig. 8.

Finally, we address the validity of performing the calculations at nonzero external fields, using the frozen zero-field structure. In Fig. 8(c), we display the band structure as a function of electric field using the PBE-D2 relaxed structure at zero field. As seen, the effect of relaxing the atoms and cell vectors at each field versus keeping them frozen at the zero-field structure results is a net change of about 20 meV in the energy gaps. This is both within the error of the numerical technique and irrelevant with respect to the larger band-gap errors that are anyway inherent in DFT. Not only are the variations in the overall structural parameters with electric field small, as noted before; even the metal-chalcogen bond length changes by less than 0.01 Å. These negligible structural deformations induced by electric fields are also consistent with our observations in our previous work on band-gap tuning in graphene and graphene/h-BN heterostructures.[39] Therefore, in this particular instance at any rate, it is entirely valid to use the relaxed zero-field atomic structure to facilitate rapid calculations at other fields.

*ashwin@engin.umass.edu
†naveh@cmu.edu
‡towe@cmu.edu

[1] J. A. Wilson and A. D. Yoffe, Adv. Phys. **18**, 193 (1969).
[2] A. Enyashin, S. Gemming, and G. Seifert, Eur. Phys. J. Spec. Top. **149**, 103 (2007).
[3] M. Bar-Sadan, I. Kaplan-Ashiri, and R. Tenne, Eur. Phys. J. Spec. Top. **149**, 71 (2007).
[4] R. Tenne and C. N. R. Rao, Philos. Trans. R. Soc. London A **362**, 2099 (2004).
[5] A. K. Geim and K. S. Novoselov, Nature Mater. **6**, 183 (2007).
[6] K. S. Novoselov, D. Jiang, F. Schedin, T. J. Booth, V. V. Khotkevich, S. V. Morozov, and A. K. Geim, Proc. Natl. Acad. Sci. USA **102**, 10451 (2005).
[7] J. N. Coleman, M. Lotya, A. O'Neill, S. D. Bergin, P. J. King, U. Khan, K. Young, A. Gaucher, S. De, R. J. Smith, I. V. Shvets, S. K. Arora, G. Stanton, H.-Y. Kim, K. Lee, G. T. Kim, G. G. Duesberg, T. Hallam, J. J. Boland, J. J. Wang, J. F. Donegan, J. C. Grunlan, G. Moriarty, A. Shmeliov, R. J. Nicholls, J. M. Perkins, E. M. Grieveson, K. Theuwissen, D. W. Mccomb, P. D. Nellist, and V. Nicolosi, Science **331**, 568 (2011).
[8] A. Ayari, E. Cobas, O. Ogundadegbe, and M. S. Fuhrer, J. Appl. Phys. **101**, 014507 (2007).
[9] K. Mak, C. Lee, J. Hone, J. Shan, and T. Heinz, Phys. Rev. Lett. **105**, 136805 (2010).
[10] B. Radisavljevic, A. Radenovic, J. Brivio, V. Giacometti, and A. Kis, Nature Nanotech. **6**, 147 (2011).
[11] A. Splendiani, L. Sun, Y. Zhang, T. Li, J. Kim, C.-Y. Chim, G. Galli, and F. Wang, Nano Lett. **10**, 1271 (2010).
[12] E. McCann, Phys. Rev. B **74**, 161403 (2006).
[13] Y. Zhang, T.-T. Tang, C. Girit, Z. Hao, M. C. Martin, A. Zettl, M. F. Crommie, Y. R. Shen, and F. Wang, Nature (London) **459**, 820 (2009).
[14] T. Ohta, A. Bostwick, T. Seyller, K. Horn, and E. Rotenberg, Science **313**, 951 (2006).
[15] F. Xia, D. B. Farmer, Y. Lin, and P. Avouris, Nano Lett. **10**, 715 (2010).
[16] Z. Yang and J. Ni, J. Appl. Phys. **107**, 104301 (2010).
[17] C.-H. Park and S. G. Louie, Nano Lett. **8**, 2200 (2008).
[18] F. Zheng, Z. Liu, J. Wu, W. Duan, and B.-L. Gu, Phys. Rev. B **78**, 085423 (2008).
[19] K. H. Khoo, M. S. C. Mazzoni, and S. G. Louie, Phys. Rev. B **69**, 201401(R) (2004).
[20] M. Ishigami, J. D. Sau, S. Aloni, M. L. Cohen, and A. Zettl, Phys. Rev. Lett. **94**, 056804 (2005).
[21] Th. Böker, R. Severin, A. Müller, C. Janowitz, and R. Manzke, Phys. Rev. B **64**, 235305 (2001).
[22] A. Klein, S. Tiefenbacher, V. Eyert, C. Pettenkofer, and W. Jaegermann, Phys. Rev. B **64**, 205416 (2001).
[23] H. Rydberg, M. Dion, N. Jacobson, E. Schröder, P. Hyldgaard, S. Simak, D. Langreth, and B. Lundqvist, Phys. Rev. Lett. **91**, 126402 (2003).
[24] W. J. Schutte, J. L. de Boer, and F. Jellinek, J. Solid State Chem. **70**, 207 (1987).
[25] T. Li and G. Galli, J. Phys. Chem. C **111**, 16192 (2007).
[26] L. F. Mattheiss, Phys. Rev. B **8**, 3719 (1973).
[27] R. Coehoorn, C. Haas, J. Dijkstra, C. J. F. Flipse, R. A. de Groot, and A. Wold, Phys. Rev. B **35**, 6195 (1987).
[28] P. D. Fleischauer, J. R. Lince, P. Bertrand, and R. Bauer, Langmuir **5**, 1009 (1989).
[29] See Supplemental Material at http://link.aps.org/supplemental/10.1103/PhysRevB.84.205325 for band structure and charge-density difference plots for $MoSe_2$, $MoTe_2$, and WS_2.
[30] R. W. Godby, M. Schlüter, and L. J. Sham, Phys. Rev. Lett. **56**, 2415 (1986).
[31] B. G. Janesko, T. M. Henderson, and G. E. Scuseria, Phys. Chem. Chem. Phys. **11**, 443 (2009).
[32] M. S. Hybertsen and S. G. Louie, Phys. Rev. B **34**, 5390 (1986).

[33]M. Shishkin and G. Kresse, Phys. Rev. B **75**, 235102 (2007).
[34]M. A. L. Marques, J. Vidal, M. J. T. Oliveira, L. Reining, and S. Botti, Phys. Rev. B **83**, 035119 (2011).
[35]*Gmelin Handbook of Inorganic and Organometallic Chemistry* (Springer-Verlag, Berlin, 1995), 8th ed., Vol. B7.
[36]A. R. Botello-Mendez, F. Lopez-Urias, M. Terrones, and H. Terrones, Nanotechnology **20**, 325703 (2009).
[37]S. Lebègue and O. Eriksson, Phys. Rev. B **79**, 115409 (2009).
[38]C. Ataca and S. Ciraci, J. Phys. Chem. C **115**, 13303 (2011).
[39]A. Ramasubramaniam, D. Naveh, and E. Towe, Nano Lett. **11**, 1070 (2011).
[40]G. Kresse and J. Furthmüller, Comput. Mater. Sci. **6**, 15 (1996); Phys. Rev. B **54**, 11169 (1996).
[41]P. E. Blochl, Phys. Rev. B **50**, 17953 (1994).
[42]G. Kresse and D. Joubert, Phys. Rev. B **59**, 1758 (1999).
[43]J. P. Perdew, K. Burke, and M. Ernzerhof, Phys. Rev. Lett. **77**, 3865 (1996).
[44]VASP manual [http://cms.mpi.univie.ac.at/vasp/vasp/].
[45]J. Neugebauer and M. Scheffler, Phys. Rev. B **46**, 16067 (1992).
[46]K. Momma and F. Izumi, J. Appl. Crystallogr. **41**, 653 (2008).
[47]S. Grimme, J. Comput. Chem. **27**, 1787 (2006).
[48]See [http:// cms.mpi.univie.ac.at / vasp / vasp / DFT_D2_method_ Grimme.html].
[49]T. Bučko, J. Hafner, S. Lebegue, and J. G. Ángýan, J. Phys. Chem. A **114**, 11814 (2010).
[50]As a check we relaxed the interplanar spacing for MoS_2 to its equilibrium value both with PBE as well as PBE with semiempirical dispersion corrections and calculated the band structure as a function of external field. While the position of the conduction band minimum is sensitive to the interlayer spacing (Ref. 25), the band gap still closes with increasing external fields. (See detailed discussion in the Appendix.)